Far-Infrared Water Line Emissions From Circumstellar Outflows

Wesley Chen and David A. Neufeld
Department of Physics & Astronomy, The Johns Hopkins University, Baltimore, MD 21218

ABSTRACT

We have modeled the far-infrared water line emission expected from circumstellar outflows from oxygen-rich late-type stars, as a function of the mass-loss rate and the terminal outflow velocity. For each mass-loss rate and terminal outflow velocity considered, we computed self-consistently the gas density, temperature, outflow velocity, and water abundance as a function of distance from the star. We then used an escape probability method to solve for the equilibrium level populations of 80 rotational states of water and thereby obtained predictions for the luminosity of a large number of far-infrared rotational transitions of water. In common with previous models, our model predicts that water will be copiously produced in the warm circumstellar gas, and that water rotational emission will dominate the radiative cooling. *However, our use of a realistic radiative cooling function for water leads to a lower gas temperature than that predicted in previous models. Our predictions for the far-infrared water line luminosities are consequently significantly smaller than those obtained in previous studies.* Observations to be carried out by the Infrared Space Observatory will provide a crucial test of the models presented here.

Subject headings: circumstellar matter - stars: late-type - stars: mass-loss

1. INTRODUCTION

Theoretical models (e.g. Goldreich & Scoville 1976, hereafter GS76) for the physical and chemical conditions in circumstellar outflows make the strong prediction that water will be copiously produced in oxygen-rich outflows; water is expected to account for almost all of the gas-phase oxygen that is not bound as CO, and far-infrared water emissions

are expected to dominate the radiative cooling of the gas (Neufeld & Kaufman 1993, hereafter NK93). This prediction is supported by observations of luminous water maser emissions from hundreds of such outflows (Bowers & Hagen 1984 and references therein), with luminosities that are broadly consistent with large water abundances (Cooke & Elitzur 1985).

Although several submillimeter water maser transitions have been detected from oxygen-rich circumstellar outflows (Menten et al. 1990a,b; Melnick et al. 1993), none of the far-infrared non-masing transitions that dominate the cooling of the gas has yet been observed, because absorption by the Earth's atmosphere makes such observations infeasible even at airplane altitude. However, the Infrared Space Observatory (ISO) satellite, scheduled for launch in 1995, should provide an ideal instrument for the study of far-infrared cooling transitions of water molecules within warm astrophysical gas.

In this *Letter*, we present new predictions for the expected far-infrared water line luminosities from oxygen-rich circumstellar outflows. In §2, we describe our treatment of the physical and chemical processes that determine the dynamics, temperature, chemical composition, and water line emissivities within such outflows. In §3 we present our results for the structure of the outflowing gas and for the far-infrared water emission line strengths. In §4, we discuss the significant differences between the results obtained here and those obtained in previous studies.

2. MODEL DESCRIPTION

2.1. Dynamics

Assuming that the circumstellar outflow is accelerated primarily by radiation pressure upon newly-formed dust grains (Gilman 1972; Salpeter 1974; Kwok 1975), we may describe the outflow velocity of the gas by the equation

$$v\frac{dv}{dr} = \frac{\kappa(r)L}{4\pi r^2 c} - \frac{GM}{r^2}, \tag{1}$$

(GS76), where $v(r)$ is the velocity of the gas at distance r from the center of the star, $\kappa(r)$ is the dust opacity, L is the stellar luminosity, c is the speed of light, and M is the mass of the star.

For simplicity, we followed GS76 in assuming that the dust opacity increases steadily with r according to the expression

$$\kappa(r) = \frac{Q n_d \sigma_d}{\rho} = \Gamma \left(1 + \frac{\Delta r^2}{[(10R)^2 + r^2]} \right), \tag{2}$$

where R is the stellar radius, Γ and Δ are constants that are determined by the initial and terminal gas outflow velocities, n_d and σ_d are the number density and typical geometrical cross section of the dust grains, and Q is the typical ratio of the infrared absorption cross section to the geometrical grain cross section. We take 0.03 as an effective value for Q, adopting the results computed by Justtanont et al. (1994; hereafter JST94) for silicate grains with a power-law size distribution (Mathis, Rumpl, & Nordsieck 1977). Given a particular value of the terminal outflow velocity, the exact dependence of κ upon r does not greatly affect the predicted strengths of the water lines considered in this *Letter*, because we have confined our attention to transitions that are primarily excited outside the region where the gas and dust are accelerated. Thus although more detailed models can be constructed for the variation of the opacity with position (e.g. JST94), the effect upon the predicted line strengths is small for the transitions considered here.

2.2. Thermal Balance

The gas temperature T in the outflow satisfies the equation

$$\frac{r}{T}\frac{dT}{dr} = -\frac{4}{3}\left(1 + \frac{1}{2}\frac{d\ln v}{d\ln r}\right) + \frac{2r(H-C)}{3 v n_{\rm H} k T (x_H + x_{H2} + x_{He})} \tag{3}$$

(GS76), where $n_{\rm H}$ is the density of hydrogen nuclei, and x_H, x_{H2}, and x_{He} are respectively the abundances of H, H_2, and He relative to hydrogen nuclei. Again following GS76, we assume $x_H = x_{H2} = \frac{1}{3}$ and $x_{He} = 0.1$, although the results depend only very weakly upon the exact values adopted. The first term on the right hand side describes the adiabatic cooling rate, and H and C are the heating and cooling rates per unit volume due to other processes.

The additional heating and cooling processes we considered are grain-gas collisional heating, H_2O rovibrational heating (resulting from the absorption of stellar radiation by water molecules), and H_2O rovibrational cooling. We have also considered CO and H_2 cooling and found them to be negligible. The grain-gas collisional heating rate is $\frac{1}{2}\rho v_d^3 \sigma_d n_d$, where v_d is the drift velocity of the dust relative to the gas. Provided v_d is much greater

than the sound speed in the gas, the drift velocity is given by $v_d = (QLv/\dot{M}c)^{1/2}$, where $\dot{M}$ is the mass loss rate (GS76; Tielens 1983). For H_2O rovibrational cooling, we used the cooling functions of NK93; the cooling rate is a function of the temperature, the gas density, and an optical depth parameter which depends on the water density and the velocity gradient in the outflow. We estimated the *heating* rate due to the absorption of stellar radiation by water molecules as

$$H_{\rm H2O} = W C_{\rm H2O}(T_*), \tag{4}$$

where $C_{\rm H2O}(T)$ is the water *cooling* rate given by NK93 for gas temperature T, where $4\pi W = 2\pi(1 - [1 - (R/r)^2]^{1/2})$ is the solid angle subtended by the star, and T_* is the temperature of the stellar photosphere, which we assume to radiate as a blackbody. This approximate expression shows the correct behavior $H_{\rm H2O} = C_{\rm H2O}$ required by thermodynamics in the limit where the gas is surrounded ($W = 1$) by radiation with a temperature equal to the gas temperature. Our present treatment of the thermal balance neglects the effects of heating that may result from the absorption of dust continuum radiation by water; based upon theoretical models for the dust continuum radiation (S. Doty 1995, private communication), we expect such effects to be important only close to the star, i.e. inside the region that gives rise to the water line emission considered in this paper.

2.3. Chemistry

For the purposes of this study, we needed only to determine the abundance of water. Accordingly, we based our computation of the abundances of the major oxygen bearing species upon a very limited chemical network. At temperatures $\gtrsim 300$ K, water is formed rapidly by the reaction sequence:

$$O + H_2 \rightleftharpoons OH + H$$

$$OH + H_2 \rightleftharpoons H_2O + H$$

The rate coefficients for these reactions have been given by Wagner and Graff (1987). Due to the endothermic nature of the first forward reaction, and the relatively high activation barrier of the second forward reaction, this reaction sequence is effective only in the warm ($T \gtrsim 300$ K) regions close to the star. Far away from the star, the H_2O and OH molecules are photodissociated by the interstellar radiation field:

$$H_2O + h\nu \rightarrow H + OH$$

$$OH + h\nu \rightarrow O + H.$$

The photodissociation rates for OH and H_2O have been calculated by Roberge et al. (1991) as a function of visual extinction within a plane-parallel slab; we have modified their results as appropriate for the spherically-symmetric geometry of relevance to circumstellar outflows. The rate equations for all these chemical processes were integrated along with equations (1) and (3) to yield the temperature, density, outflow velocity and chemical abundances as a function of r.

2.4. H_2O line emission

Once the temperature, density, velocity, and abundance profiles were computed, we used an escape probability method (NK93) to obtain the rotational level populations of water and the water line emissivities as a function of r. Integrating the line emissivities over the entire outflow region, we obtained the luminosity for each water transition.

Our present treatment of the water line emission neglects the effects of radiative pumping by dust continuum radiation; as in §2.2, we expect such effects to be unimportant in the region that gives rise to the water line emission considered in this paper. We defer to a future paper a more complete analysis in which the line radiation, dust continuum radiation and thermal balance are treated entirely self-consistently by an iterative method; such a calculation will be needed to obtain reliable predictions for water transitions of higher excitation than those considered here.

3. RESULTS

Figures 1, 2, and 3 describe the structure of the outflow region for the same set of parameters considered by GS76: stellar mass $M = 2 \times 10^{33}$ g; stellar luminosity $L = 4 \times 10^{37}$ erg s^{-1}; stellar radius $R = 6 \times 10^{13}$ cm; stellar temperature $T_* = 2000$ K; mass outflow rate $\dot{M} = 3 \times 10^{-5} M_\odot \mathrm{yr}^{-1}$; terminal outflow velocity $v_\infty = 20$ km s^{-1}; and initial oxygen abundance $n(O)/n_H = 5 \times 10^{-4}$.

Figure 1 shows the strength of various cooling and heating processes as a function of the distance r from the star. The heating is dominated by the dust-gas collision process except close to the star where water vibrational heating is important. The water rotational

cooling rate drops rapidly between $r = 10^{16}$ and $r = 10^{17}$ cm due to the photodissociation of H_2O molecules by the interstellar UV field. The effects of photodissociation are also apparent in Figure 2, which shows the abundances of O, OH and H_2O. For $r < 3 \times 10^{16}$ cm, photodissociation is negligible and H_2O accounts for almost all the gas-phase oxygen that is not bound as CO. The resultant temperature profile is shown in Figure 3, together with the analogous result from GS76.

Example line strengths are given in Table 1 for three different mass-loss rates. Here we compare the far-infrared line strengths predicted by our model with those obtained previously by Deguchi and Rieu (1990; hereafter DR90), *who assumed the GS76 temperature profile in their calculation.* These results apply to a the same terminal outflow velocity ($v_\infty = 10$ km s^{-1}) and the same initial oxygen abundance ($n(O)/n(H_2) = 4 \times 10^{-4}$) assumed by DR90 for the case $\dot{M} = 10^{-5} M_\odot \mathrm{yr}^{-1}$. Table 1 lists the predicted fluxes for seven transitions of ortho-water for which ISO observations are planned, given an assumed distance to the star of 100 pc. The final column in Table 1 shows the ratio of our calculated fluxes for $\dot{M} = 10^{-5} M_\odot \mathrm{yr}^{-1}$ to those obtained by DR90. As expected given the lower gas temperatures predicted in the present study (see Figure 3), our predicted line strengths are smaller than those of DR90 by substantial factors (ranging from 7 to 24).

In Figure 4, we examine the dependence of the far-infrared water line luminosities upon the assumed abundance of gas-phase oxygen not bound as CO (or, equivalently, upon the assumed water abundance). The results shown here apply to the outflow from the star IRC+10011, given the following assumed parameters (Knapp & Morris 1985, JST94): stellar mass $M_* = 1\, M_\odot$, mass loss rate $\dot{M} = 1 \times 10^{-5} M_\odot \mathrm{yr}^{-1}$, stellar temperature $T_* = 2000K$, stellar radius $R = 4.5 \times 10^{13}$ cm, terminal outflow velocity $v_\infty = 23$ km s^{-1}, and distance to the star = 480 pc. For most of the emission line strengths shown in Figure 4, there is no strong dependence upon the water abundance, because water is the dominant coolant. Thus an increase in the assumed water abundance leads to an decrease in the gas temperature so that the net rate of water emission remains unchanged. Furthermore, much of the emission is generated within regions where the lines are optically thick.

4. DISCUSSION

Our predicted line strengths for far-infrared water emissions from oxygen-rich circumstellar outflows are substantially smaller than those obtained previously by DR90. This discrepancy arises because our model predicts a gas temperature in the outflow which is much smaller than that obtained by GS76. The lower temperature obtained in the

present study has two origins. First, as noted by JST94, GS76 adopted an unrealistically large value of 0.5 for Q, the typical ratio of the infrared absorption cross section to the geometrical grain cross section. This in turn led to overestimates of the grain drift velocity v_d and of the gas-grain collisional heating rate. Using the more realistic value $Q = 0.03$, which we adopt in the present study, JST94 obtained a gas temperature in the outflow which was considerably smaller than that of GS76. Second, the simple three-level model for the water molecule adopted by both GS76 and JST94 leads to an estimate of the water cooling rate which lies significantly *below* the more realistic cooling function derived by NK93.

Observations of water maser emission from circumstellar outflows may provide additional support for the lower outflow temperatures that we derive. Theoretical models for such emission, constructed by Cooke & Elitzur (1985) (and subsequently by Neufeld & Melnick 1991) *on the basis of the GS76 temperature profile*, predicted maser luminosities for high mass-loss rate outflows that significantly exceed what is observed in any real source. Cooke & Elitzur (1985) suggested that their neglect of photodissociation might have led to an overestimate of the maser luminosity. We regard that explanation as unlikely, since for mass loss rates in excess of $\dot{M} = 3 \times 10^{-5} M_{\odot} \mathrm{yr}^{-1}$, water is significantly photodissociated only at radii $\gtrsim 10^{16}$ cm whereas the maser emission is generated within a region of radius $\sim 10^{15}$ cm. We speculate instead that previous theoretical models overestimated the maser line luminosity because they were based upon an overestimate of the gas temperature in the outflowing gas. The inclusion of maser transitions in our model will be needed to test this speculation.

We thank S. Doty for providing us with estimates for the dust continuum radiation field in IRC+10011, and we gratefully acknowledge the support of NASA grant NAGW-3147 from the Long Term Space Astrophysics Research Program and of NASA grant NAGW-3183.

Table 1: Predicted Emission Line Fluxes and Comparison to DR90 Results

Transition	Wavelength	Line Flux (W cm^{-2})[a]			CN/DR ratio[b]
	(μm)	$\dot{M} = 10^{-4}$	$\dot{M} = 10^{-5}$	$\dot{M} = 10^{-6}$	for $\dot{M} = 10^{-5}$
$2_{12} - 1_{01}$	179.5265	2.1×10^{-19}	1.9×10^{-19}	1.2×10^{-19}	0.071
$3_{30} - 3_{21}$	136.4944	2.0×10^{-19}	5.9×10^{-20}	1.7×10^{-20}	—- [c]
$4_{14} - 3_{03}$	113.5366	3.6×10^{-19}	1.6×10^{-19}	9.5×10^{-20}	0.043
$2_{21} - 1_{10}$	108.0730	4.3×10^{-19}	2.3×10^{-19}	1.2×10^{-19}	0.052
$2_{20} - 1_{11}$	100.983	4.7×10^{-19}	2.1×10^{-19}	6.8×10^{-20}	0.15
$5_{05} - 4_{14}$	99.4926	4.3×10^{-19}	1.6×10^{-19}	7.8×10^{-20}	0.041
$5_{15} - 4_{04}$	95.6261	4.2×10^{-19}	1.4×10^{-19}	5.1×10^{-20}	0.11
$6_{16} - 5_{05}$	82.0304	5.0×10^{-19}	1.7×10^{-19}	7.3×10^{-20}	0.055

[a] Line flux for a terminal outflow velocity $v_\infty = 10\,\mathrm{km\,s^{-1}}$, a water abundance $n(H_2O)/n(H_2) = 4 \times 10^{-4}$, and an assumed distance to the source of 100 pc.

[b] Ratio of the results of this study (CN) to those of DR90 (DR).

[c] Transition not listed by DR90

REFERENCES

Bowers, P.F., & Hagen, W. 1984, ApJ, 285, 637
Cooke, B., & Elitzur, M. 1985, ApJ, 295, 175
Deguchi, S., & Q-Rieu, N. 1990, ApJ, 360, L27 (DR90)
Gilman, R. C. 1972, ApJ, 178, 423
Goldreich, P., & Scoville, N. 1976, ApJ, 205, 144 (GS76)
Justtanont, K., Skinner, C. J., & Tielens, A. G. G. M. 1994, ApJ, 435, 852 (JST94)
Knapp, G. R., & Morris, M. 1985, ApJ, 292, 640
Kwok, S. 1975, ApJ, 198, 583
Mathis, J. S., Rumpl, W., & Nordsieck, K. H. 1977, ApJ, 217, 425
Menten, K. M., Melnick, G. J., & Phillips, T. G. 1990a, ApJ, 350, L41
Menten, K. M., Melnick, G. J., Phillips, T. G., & Neufeld, D. A. 1990b, ApJ, 363, L27
Melnick, G. J., Menten, K. M., Phillips, T. G. & Hunter, T. 1993, ApJ, 416, L37
Neufeld, D. A., & Melnick, G. J. 1991, ApJ, 368, 215
Neufeld, D. A., & Kaufman, M. J. 1993, ApJ, 418, 263 (NK93)
Roberge, W. G., Jones, D., Lepp, S., & Dalgarno, A. 1991, ApJS, 77, 287
Salpeter, E. E. 1974, ApJ, 193, 585
Tielens, A. G. G. M. 1983, ApJ, 271, 702
Wagner, A. F. & Graff, M. M. 1987, ApJ, 317, 423

FIGURE CAPTIONS

FIGURE 1: The heating and cooling rates for various processes, as a function of distance r from the star, for the set of outflow parameters adopted by GS76 (see text).

FIGURE 2: The abundances of O, OH and H_2O relative to hydrogen nuclei, as a function of distance from the star, for the set of outflow parameters adopted by GS76 (see text).

FIGURE 3: Gas temperature, as a function of distance r from the star, for the set of outflow parameters adopted by GS76 (see text). The GS76 temperature profile is shown for comparison.

FIGURE 4: Predicted emission line fluxes for the outflow from IRC+10011, as a function of the assumed water abundance. The assumed outflow parameters are given in the text.

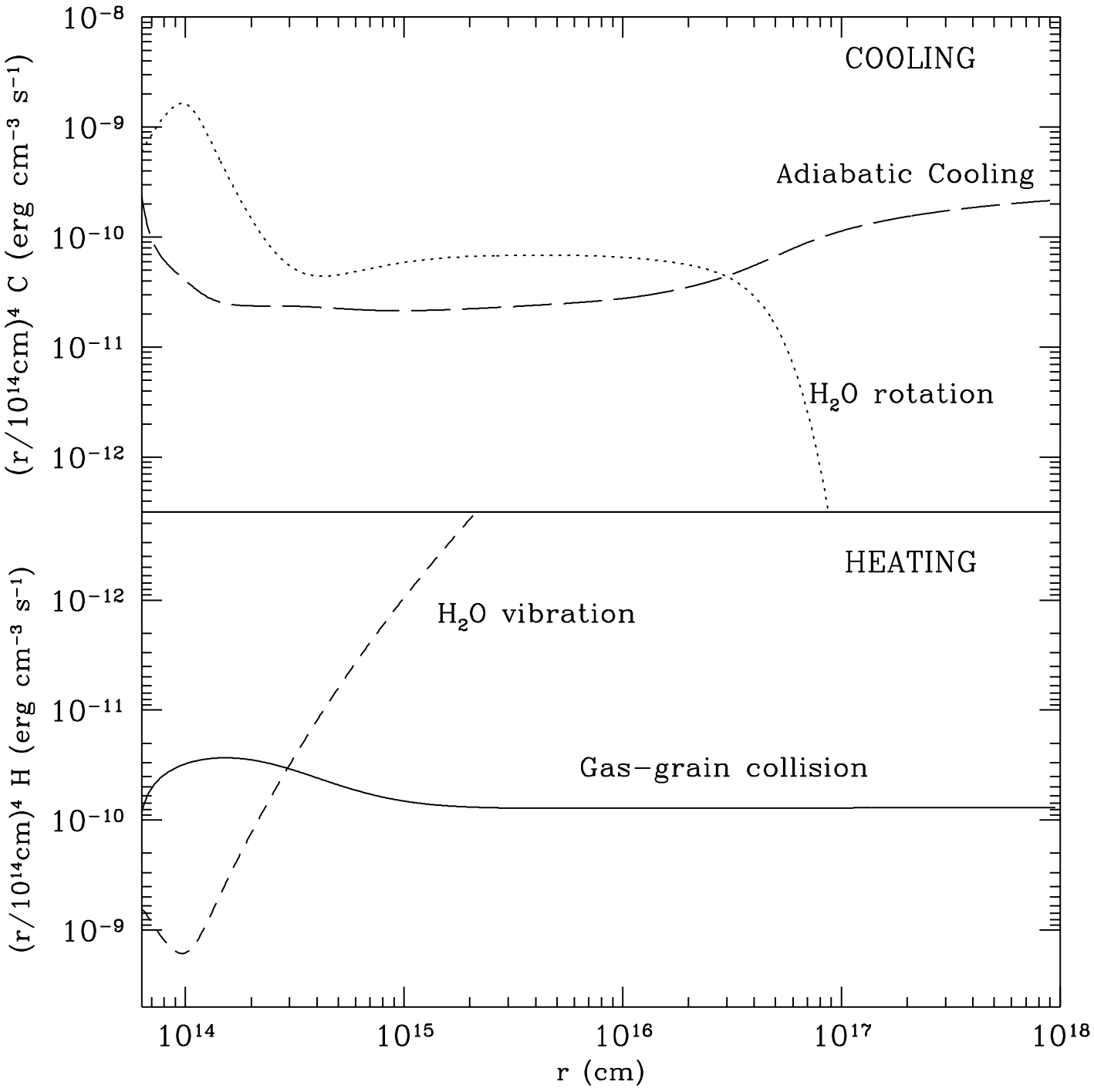
COOLING
Adiabatic Cooling
H2O rotation
HEATING
H2O vibration
Gas−grain collision
(r/10^14cm)^4 C (erg cm^-3 s^-1)
(r/10^14cm)^4 H (erg cm^-3 s^-1)
r (cm)
10^-8
10^-9
10^-10
10^-11
10^-12
10^14
10^15
10^16
10^17
10^18

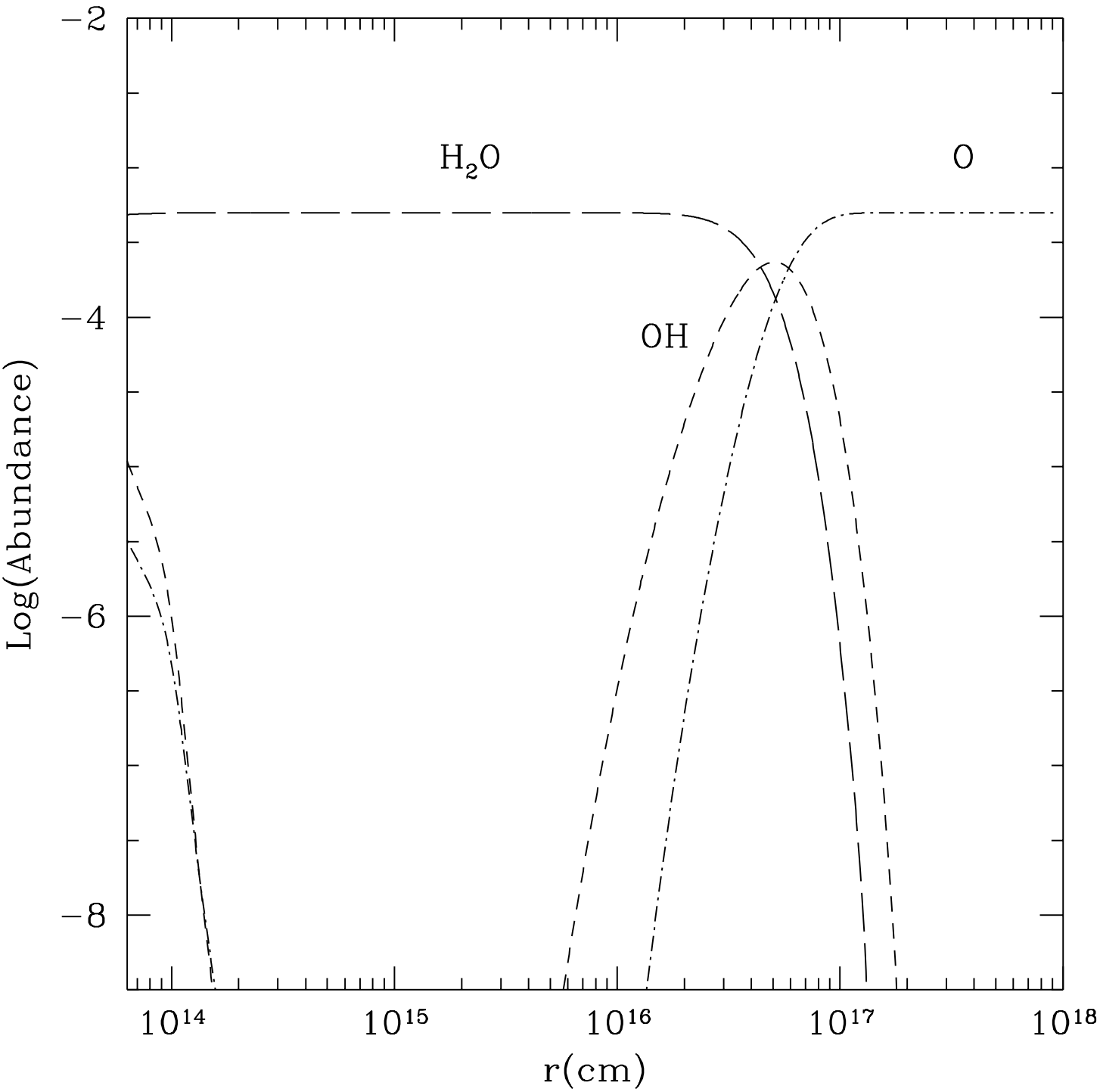
−2
−4
−6
−8
Log(Abundance)
H2O
O
OH
10^14
10^15
10^16
10^17
10^18
r(cm)

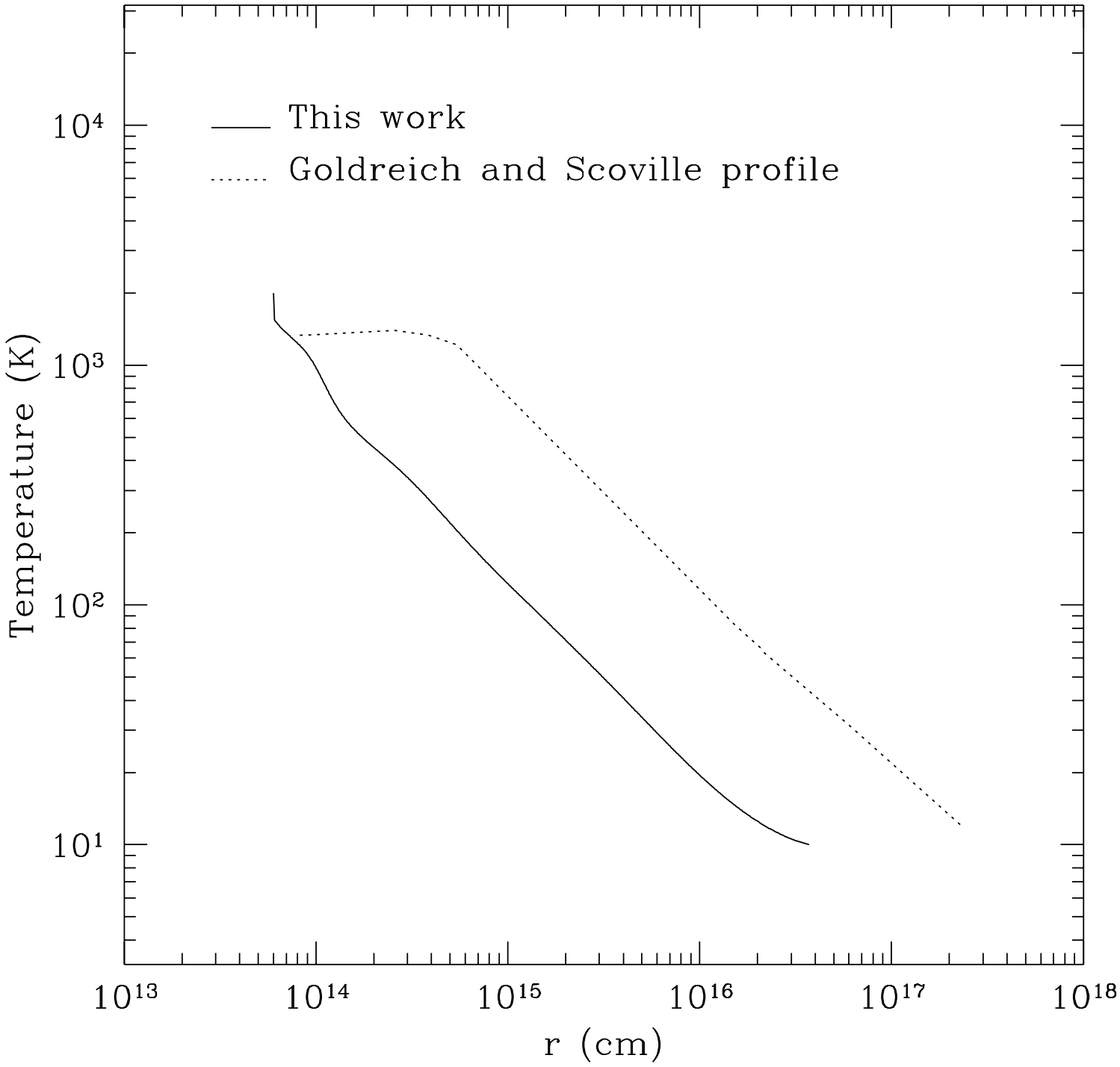
This work
Goldreich and Scoville profile
Temperature (K)
10^4
10^3
10^2
10^1
10^{13}
10^{14}
10^{15}
10^{16}
10^{17}
10^{18}
r (cm)

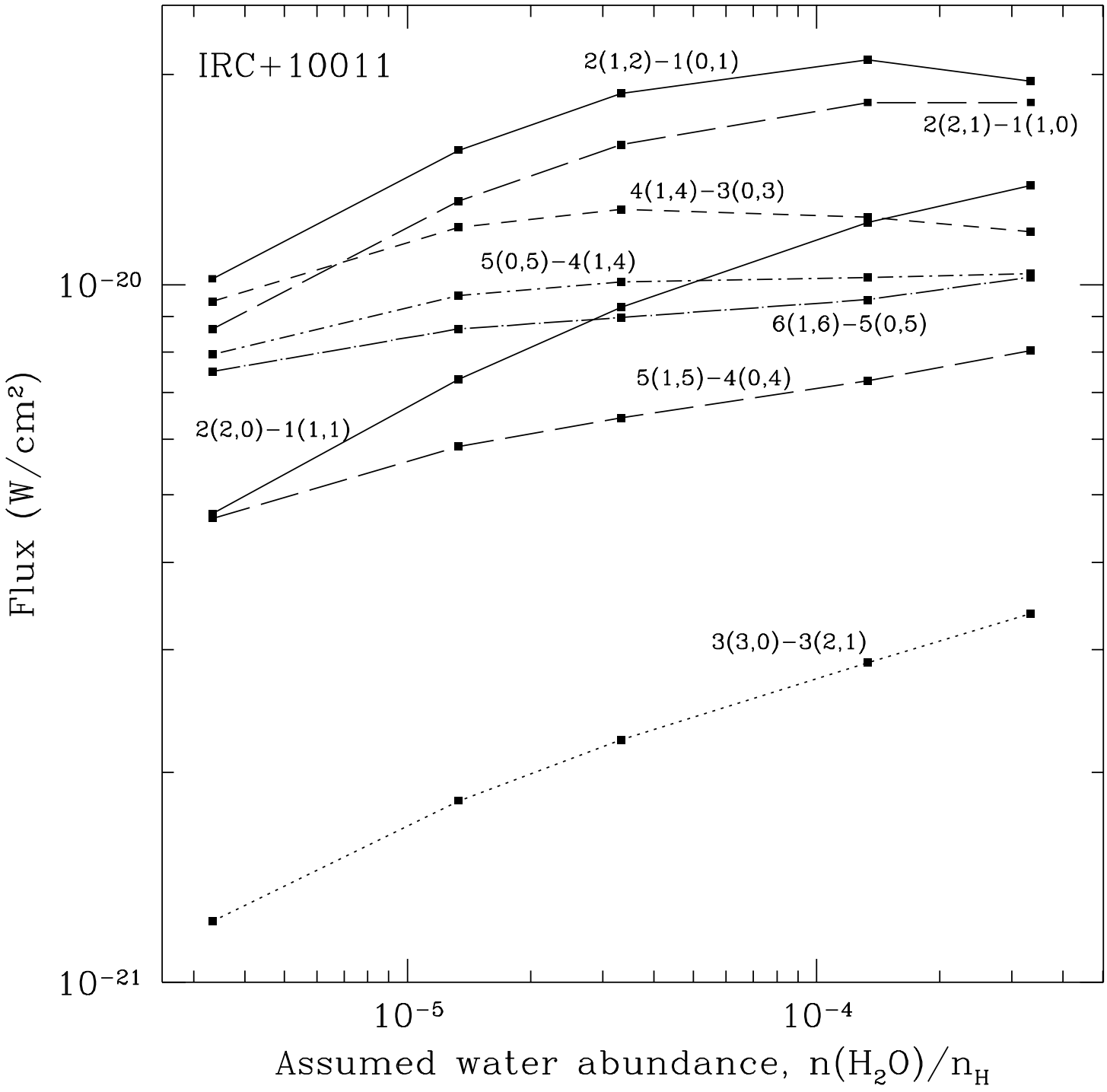
IRC+10011
2(1,2)−1(0,1)
2(2,1)−1(1,0)
4(1,4)−3(0,3)
5(0,5)−4(1,4)
6(1,6)−5(0,5)
5(1,5)−4(0,4)
2(2,0)−1(1,1)
3(3,0)−3(2,1)
10^−20
10^−21
10^−5
10^−4
Flux (W/cm^2)
Assumed water abundance, n(H2O)/nH